

Supporting information

High Pressure Ammonia decomposition on Ru-K/CaO catalysts

Salvador Sayas,^a Natalia Morlanés,^a Sai P. Katikaneni,^b Aadesh Harale,^b Bandar Solami,^b Jorge Gascon^{*a}

^aKAUST Catalysis Center (KCC), King Abdullah University of Science and Technology (KAUST), Thuwal 23955-6900, Saudi Arabia

^bCarbon Management R&D Division, Research and Development Center, Saudi Aramco, Dhahran, Saudi Arabia 31311

Mass and heat transport limitations

Several experiments were performed in order to confirm the reaction rates provided along the manuscript are not affected by diffusional heat and mass transport limitations.

The catalyst 3%Ru-10%K/CaO was used for the experiments. First, a set of experiments were performed in order to discard intraparticle mass diffusional limitations by using different particle sizes of the catalyst, while the rest of operating conditions were kept constant. 200 mg of catalysts were pelletized recrushed and sieved into controlled size particles in three ranges: 1) between 100 μm and 350 μm , 2) between 350 μm and 500 μm and 3) between 500 μm and 700 μm ; the catalyst was diluted with 1g (500 μm) of SiC for all experiments. The catalytic performance was evaluated under similar reaction conditions: atmospheric pressure, temperature in the range 250-450 °C and space velocity $\text{WHSV}=9000 \text{ mL g}_{\text{cat}}^{-1} \text{ h}^{-1}$ by using 30 mL min^{-1} ammonia. Prior to the activity measurement, the catalysts were activated in situ with hydrogen (25 mL min^{-1}) at 500°C for 3h. The results of ammonia conversion related to this set of experiments to discard intraparticle mass transfer limitations, are shown in Figure S1.

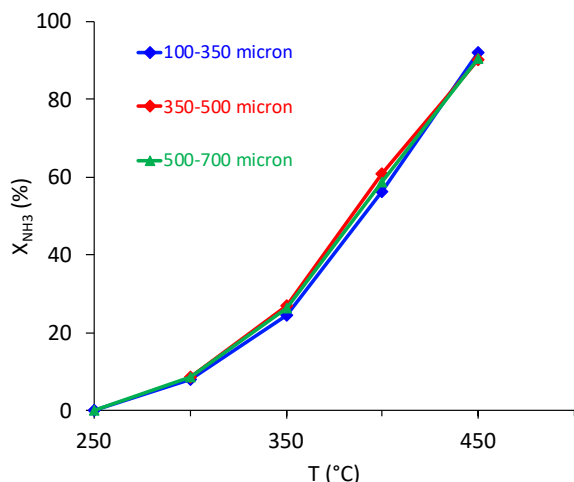


Table S1. Ammonia conversion at constant space velocity over for 3%Ru-10%K/CaO, using controlled particle sizes in different ranges to discard intraparticle mass transfer limitations. Reaction conditions: P=1 atm; T=300-450°C; NH_3 flow rate 30 mL min^{-1} ; WHSV : 9000 $\text{mL g}^{-1} \text{ h}^{-1}$

Particle size	300 °C	350 °C	400 °C	450 °C
100-350 μm	8.1	24.4	56.2	91.9
350-500 μm	8.5	27.1	60.9	90.2
500-700 μm	8.6	26.4	58.8	90.4

Figure S1. Experiments to discard intraparticle mass transfer limitations. Ammonia conversion versus temperature for 3%Ru-10%K/CaO catalyst. Reaction conditions P=1 atm; T=250-450°C; NH_3 flow rate 30 mL min^{-1} ; WHSV : 9000 $\text{mL g}^{-1} \text{ h}^{-1}$

Second, a set of experiments was performed in order to discard external particle mass transport limitations by using different ammonia flow rates and catalyst loadings while keeping always the same space velocity $\text{WHSV}=9000 \text{ mL g}_{\text{cat}}^{-1} \text{ h}^{-1}$. The ammonia flow rate was modified in the range 15-75 mL min^{-1} , and the catalyst load accordingly, in the range 100-500 mg. The amount of SiC used in each

experiment was changed in order to always keep the ratio 10/2 of SiC/catalyst. The rest of operating conditions were kept constant, with temperature in the range 250-450 °C. Prior to the activity measurement, the catalysts were activated in situ with hydrogen (25 mL min⁻¹) at 500°C for 3h. The conversion results of this set of experiments is shown in Figure S2.

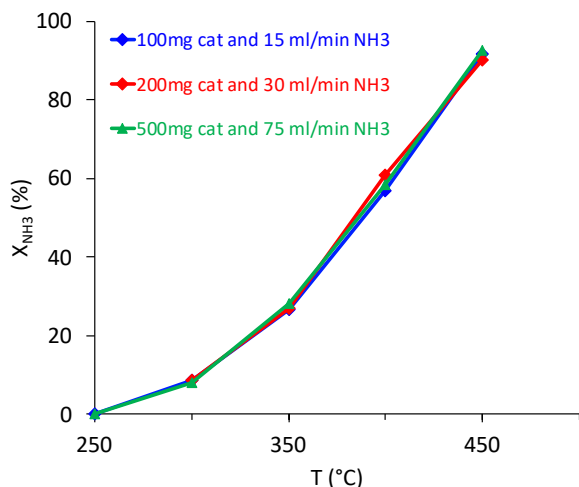


Table S2. Ammonia conversion at constant space velocity over for 3%Ru-10%K/CaO, using increasing catalyst load and ammonia flow rate, to discard external mass transfer limitations. Reaction conditions: P=1 atm; T=300-450°C; NH₃ flow rate 30 mL min⁻¹; WHSV: 9000 mL g⁻¹ h⁻¹

Catalyst - NH ₃ flow rate (mg) (mL min ⁻¹)	300 °C	350 °C	400 °C	450 °C
100 mg - 15 mL min ⁻¹	8.5	26.7	56.9	91.7
200 mg - 30 mL min ⁻¹	8.5	27.1	60.9	90.2
500 mg - 75 mL min ⁻¹	8.1	28.2	58.3	92.7

Figure S2. Experiments to discard external mass transfer limitations. Ammonia conversion versus temperature for 3%Ru-10%K/CaO catalyst. Reaction conditions: P=1 atm; T=250-450°C; NH₃ flow rate 30 mLmin⁻¹; WHSV: 9000 mL g⁻¹h⁻¹

Third, a set of experiments was performed in order to discard heat transfer limitations by using different ratios catalyst/SiC, while the rest of operating conditions were kept constant. Three different experiments using 200/500, 200/1000 and 200/4000 for the ratio mg catalyst/mg SiC. The catalytic performance was evaluated under same reaction conditions: atmospheric pressure, temperature in the range 250-450 °C and space velocity WHSV=9000 mL g_{cat}⁻¹ h⁻¹ by using 30 mL min⁻¹ ammonia. Prior to the activity measurement, the catalysts were activated in situ with hydrogen (25 mL min⁻¹) at 500°C for 3h. The results of this set of experiments is shown in Figure S3.

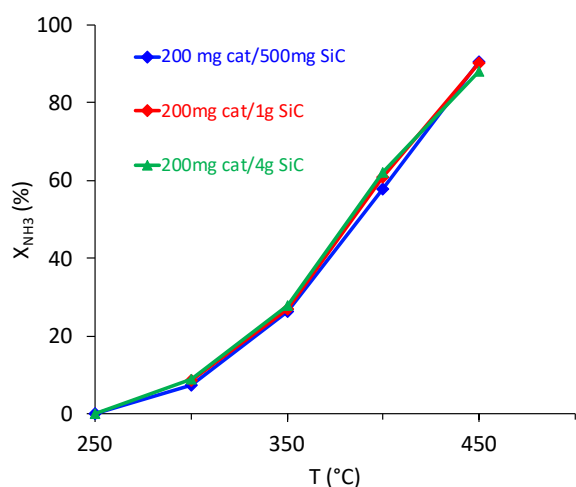


Table S3. Ammonia conversion at constant space velocity over for 3%Ru-10%K/CaO, using increasing diluent silicon carbide (SiC), to discard heat transfer limitations. Reaction conditions: P=1 atm; T=300-450°C; NH₃ flow rate 30 mL min⁻¹; WHSV: 9000 mL g⁻¹ h⁻¹

Catalyst / SiC	300 °C	350 °C	400 °C	450 °C
200 mg / 500mg	7.4	26.4	57.8	90.4
200mg / 1g	8.5	27.1	60.9	90.2
200mg / 4g	8.9	27.8	62.2	88.0

Figure S3. Experiments to discard heat transfer limitations. Ammonia conversion versus temperature for 3%Ru-10%K/CaO catalyst. Reaction conditions: P=1 atm; T=250-450°C; NH₃ flow rate 30 mL min⁻¹; WHSV: 9000 mL g⁻¹ h⁻¹

The results from this set of experiments confirms that reported reaction data were obtained in the kinetic regime and no mass or heat transfer limitation exist under the reaction conditions explored here. For all these experiments, each set of conditions were kept at each temperature for 1 hour, and the conversion shown in the graphs is the average obtained from the 20 chromatographic analysis.

Comparison Ru particle size observed by TEM and CO chemisorption.

Table S4. Ruthenium particle sizes for Ru-based catalysts.

Sample	$d_p(\text{nm})$	
	CO chemisorption	Average TEM
1%Ru10%K/CaO	6	-
2%Ru10%K/CaO	6	-
3%Ru10%K/CaO	6	7
5%Ru10%K/CaO	11	-
7%Ru10%K/CaO	17	-
3%Ru/CaO	9	9
3%Ru5%K/CaO	8	-
3%Ru15%K/CaO	6	-

Kinetic studies

The Arrhenius plots for the Ru-K/CaO catalysts with different Ru and K loadings, are shown in Figures S4 and S5. The reaction rates were calculated from the ammonia conversion values assuming a differential reactor. The activation energies were calculated from the slope of the $\ln(\text{rate})$ vs. $1/T$ plots.

In Figure S4, no significant change in the activation energies is observed for the catalysts with different Ru loading; while for the catalysts with different K loading, clearly the activation energy decreases upon increasing K loading. Figure S5 shows no effect of the operating pressure in the activation energy in the range 1-40 bar explored here.

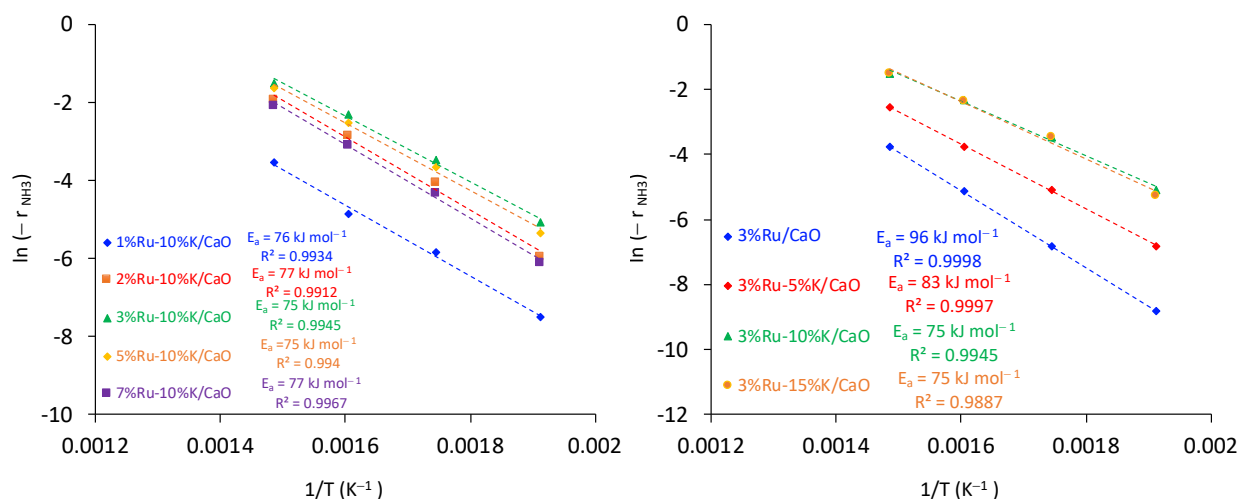


Figure S4. Arrhenius plots in the temperature range 250-400 °C for RuK/CaO catalysts; effect of Ru and K loadings. Reaction conditions: P_{atm} , NH_3 flow rate 30 ml/min and WHSV: 9000 mL g⁻¹ h⁻¹

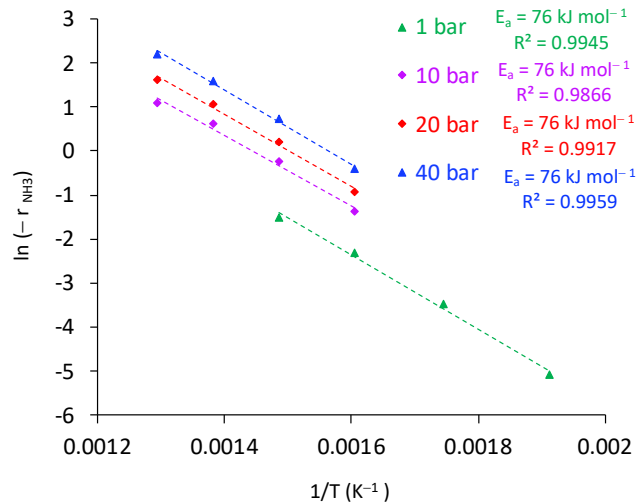


Figure S5. Arrhenius plots in the temperature range 250-400 °C for 3%Ru-10%K/CaO catalyst; effect of Pressure in the range 1-40 bar; NH₃ flow rate 30 ml/min and WHSV: 9000 mL g⁻¹ h⁻¹

The kinetic analysis was performed for the samples with and without potassium, 3%Ru-10%K/CaO and 3%Ru/CaO, respectively. Figure S6 shows the activation energies for both catalysts, the reaction orders with respect to ammonia and hydrogen and the relationship between conversion and space velocity in the range WHSV=9000-30000 mL g_{cat}⁻¹ h⁻¹, changing the ammonia flowrate in the range 30-100 mL min⁻¹. The reaction rates were calculated from the ammonia conversion values considering a differential reactor. Different partial pressures of both reactant and products were used in order to obtain the reaction orders for NH₃, H₂ and N₂, the results are plotted in Figure S6. The reaction conditions used are a total flow rate of 30 ml min⁻¹ of mixed gas (NH₃, N₂, H₂, Ar), at atmospheric pressure and 350°C. The reaction order with respect to NH₃ was obtained by changing the flow rate in the range 5-30 ml min⁻¹ and Ar balance. For the H₂ order, the NH₃ flow rate was 7.5 ml min⁻¹ kept constant, and the flow rate of H₂ in the range 5-22.5 ml min⁻¹ with Ar balance. For the N₂ order, the NH₃ flow rate was 22.5 ml min⁻¹ (kept constant), and the flow rate of N₂ in the range 1-7.5 ml min⁻¹ with Ar balance. Reaction order for nitrogen was found to be zero for both catalysts explored (not shown).

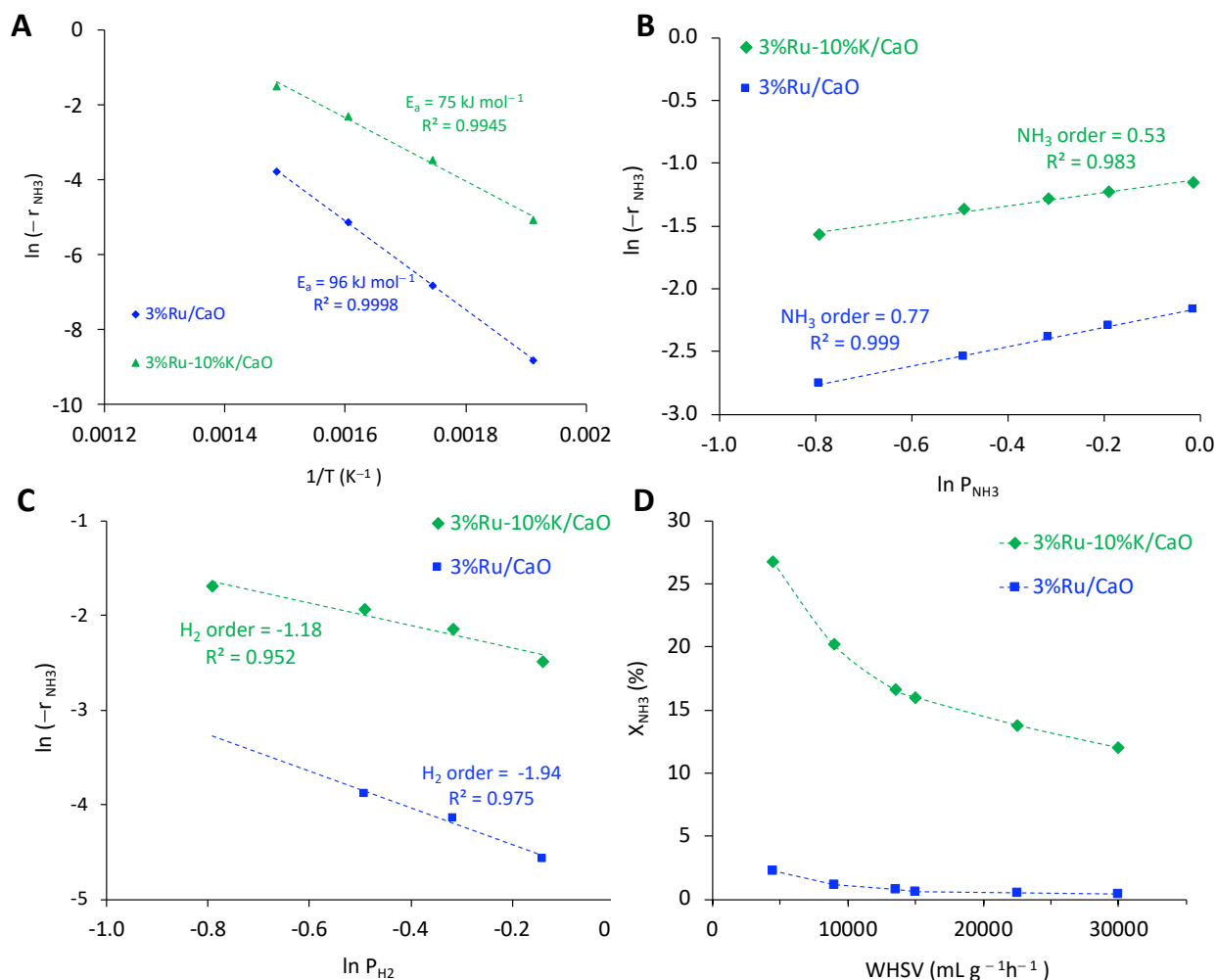


Figure S6. Kinetic parameters of the Ru-K/CaO catalysts. (A) Arrhenius plots in the temperature range 250-400 °C, at atmospheric pressure. Dependences of NH_3 -decomposition rate on the partial pressures of NH_3 (B) and H_2 (C) and Conversion vs. contact time (D) at 350 °C P_{atm} . Reaction Rate ($-r_{\text{NH}_3}$) in $\text{mol g}^{-1} \text{h}^{-1}$.

Kinetic analysis of ammonia decomposition in an integral reactor

The main goal is to develop a reliable kinetic model able to predict the performance obtained using integral reactors, under relevant reaction conditions for the industrial application of this process, when almost complete NH_3 conversion is achieved and high hydrogen concentrations at the exit of the reactor are obtained. The operating conditions, mainly the gas composition, are very different along the reactor, and the temperatures needed to attain such large conversions are usually high.

Considering the inhibition of the decomposition rate by the hydrogen produced, an integral reactor that considers the hydrogen concentration at different conversion levels along the catalytic bed must be considered in this case.

Apart from the power law given by eq. S1, and eq S2 that consider the approximation to the equilibrium, other kinetic models have been considered based on the reaction mechanism and assuming different rate determining steps.

$$(-r_{\text{NH}_3}) = k \times P_{\text{NH}_3}^a P_{\text{H}_2}^b$$

eq.S1

$$(-r_{NH_3}) = k \times P_{NH_3}^a P_{H_2}^b \left(1 - \frac{1}{K_{eq}} \left(\frac{P_{N_2} P_{H_2}^3}{P_{NH_3}^2} \right) \right) \quad \text{eq.S2}$$

All details on the development of the kinetic equations explored here can be found in the Armenise work on ammonia decomposition in an integral reactor.¹

Ammonia decomposition is known to proceed by ammonia chemisorption on the catalyst surface followed by stepwise dehydrogenation. Then, recombination of two N or two H to form N₂ and H₂, respectively, followed by desorption of the reaction products. It is assumed that the surface sites are energetically homogeneous and the adsorption of all the species follows the Langmuir isotherm. This mechanism can be described according to the following sequence of elementary reactions:

- (i) NH₃ ↔ NH₃*
- (ii) NH₃* ↔ NH₂* + H*
- (iii) NH₂* ↔ NH* + H*
- (iv) NH* ↔ N* + H*
- (v) 2N* ↔ N₂ + 2*
- (vi) 2H* ↔ H₂ + 2*

In spite of the research developed over decades into this reaction, there is no agreement about which step(s) are the RDSs, or even whether there is a single RDS, and about the surface species that are kinetically relevant. Reviewing the literature, the RDS commonly considered for this process are:

- Case A: the reaction rate is controlled by the desorption of adsorbed nitrogen atoms, and the remaining steps are in equilibrium
- Case B: the first dissociation of adsorbed NH₃ with scission of the N–H bond is the controlling step

For the case A, the reaction rate would be given by equation S3.

$$(-r_{NH_3}) = k_v [N^*]^2 - k'_v P_{N_2} [N^*]^2 \quad \text{eq.S3}$$

For the case B, the reaction rate would be given by equation S4.

$$(-r_{NH_3}) = k_{ii} [NH_3^*] [H^*] - k'_{ii} [NH_2^*] [H^*]^2 \quad \text{eq.S4}$$

where k_v and k_{ii} are the kinetics constants of the direct and reverse (k'_v and k'_{ii}) reactions of the steps (v) and (ii), in the sequence of the elementary steps provided above.

In order to obtain the kinetic equations, one step is considered to be the RDS and the rest are assumed to be in equilibrium. The kinetic models developed from this sequence of elementary step, are based on the Langmuir isotherm, and consider that all the adsorbed species can be kinetically relevant, and that the slow step can be partially reversible, and that the surface is considered ideal and energetically uniform.

Case A (**RDS: desorption of adsorbed nitrogen**), the reaction rate is given by eq. S5. A simplified equation (eq.S6) can be further developed by considering N* and H* as the most relevant species.

$$(-r_{NH_3}) = \frac{k_A K_{NH_3}^2 P_{NH_3}^2}{\left(K_{H_2}^{3/2} P_{H_2}^{3/2} (1 + \sqrt{K_{H_2} P_{H_2}}) + K_{NH_3} P_{NH_3} \left(1 + \frac{\sqrt{K_{H_2} P_{H_2}}}{K_3} \left(1 + \frac{\sqrt{K_{H_2} P_{H_2}}}{K_2} \left(1 + \frac{\sqrt{K_{H_2} P_{H_2}}}{K_1} \right) \right) \right) \right)^2} \quad \text{eq. S5}$$

$$(-r_{NH_3}) = \frac{k_A K_{NH_3}^2 P_{NH_3}^2}{\left(K_{NH_3} P_{NH_3} + K_{H_2}^{3/2} P_{H_2}^{3/2} (1 + \sqrt{K_{H_2} P_{H_2}}) \right)^2} \quad \text{eq.S6}$$

case B (RDS: first dissociation of adsorbed NH₃ with scission of the N–H bond) the reaction rate is given by eq. S7. A simplified equation (eq.S8) can be further developed by considering NH₃* N* and H* as the most relevant species.

$$(-r_{NH_3}) = \frac{k_B K_{NH_3} P_{NH_3}}{\left(1 + K_{NH_3} P_{NH_3} + \sqrt{K_{H_2} P_{H_2}} + \sqrt{K_{N_2} P_{N_2}} \left(1 + \frac{\sqrt{K_{H_2} P_{H_2}}}{K_3} \left(1 + \frac{\sqrt{K_{H_2} P_{H_2}}}{K_2}\right)\right)\right)^2} \quad \text{eq.S7}$$

$$(-r_{NH_3}) = \frac{k_B K_{NH_3} P_{NH_3}}{\left(1 + K_{NH_3} P_{NH_3} + \sqrt{K_{H_2} P_{H_2}} + \sqrt{K_{N_2} P_{N_2}}\right)^2} \quad \text{eq. S8}$$

The dependence with the temperature of the rate constants and adsorption constants in the previous kinetic equations is considered by the Arrhenius and Van't Hoff laws, given by eq. S9 and S10, respectively.

$$k_i = k_{i,0} \exp(-E_a/RT) \quad \text{eq. S9}$$

$$K_i = K_{i,0} \exp(-Q_i/RT) \quad \text{eq. S10}$$

The net reaction rates have been calculated by introducing the term into the previous equations (eq.S5 - eq.S8), that considers the approximation to the thermodynamic equilibrium (eq. S11) and accounts the reverse reaction contribution.

$$\text{Net Rate: } (-r_{NH_3}) \times \left(1 - \frac{1}{K_{eq}} \left(\frac{P_{N_2} P_{H_2}^3}{P_{NH_3}^2}\right)\right) \quad \text{eq. S11}$$

The equilibrium constant, K_{eq} , of the ammonia decomposition reaction, can be calculated (eq. S12) from the thermodynamic data,^{1,2} The values of ΔG can be estimated using eq. S13 for the operation temperature.

$$K_{eq} = \left(\frac{P_{N_2} P_{H_2}^3}{P_{NH_3}^2}\right)_{eq} = \exp\left(-\frac{\Delta G}{RT}\right) \quad \text{eq. S12}$$

$$\Delta G = 95117 - 193.67T - 0.035293T^2 + 9.22 \times 10^{-6}T^3. \quad \text{eq. S13}$$

The integration of the eq. S14 allows the calculation of the ammonia conversion for an integral reactor, where the reaction rate ($-r_{NH_3}$), is given by the kinetic models given by eq. S2, and eq. S5-S8. The calculated values of the ammonia conversion can be compared with the experimental ones, in order to optimize the parameters of each kinetic model by minimizing the sum of the squared residuals (SSR), given by eq. S15. The variance of the error for each model was also calculated according to the eq. S16, the best model will be the one that provides the lower value of the Variance of error.

$$W/F = \int_0^X \frac{dX_{NH_3}}{(-r_{NH_3})} \quad \text{eq. S14}$$

$$SSR = \min \sum_{i=1}^n (X_{NH_3}^{exp} - X_{NH_3}^{calc})^2 \quad \text{eq. S15}$$

$$\text{Var (SSR)} = \sqrt{\frac{SSR}{n-p}} \quad \text{eq. S16}$$

The parameters for the kinetic models (eq. S5-S8), including the power-law model (eq S2), were obtained by fitting the experimental values of the ammonia conversion at atmospheric pressure in a wide range of reaction conditions (T, W/F and P_{NH_3} , P_{H_2}), in order to minimize the SRR.

The available data of ammonia conversion at in a wide range of operating conditions, used for the fittings, was described above in the present document (shown in Figure S6) to explore the effect of the temperature, partial pressure of reactants and products and contact time or space velocity.

The parity plots comparing the experimental and calculated ammonia conversion values with all the kinetic models selected in this work is shown in Figure S7. Tables S4-S8 show the all parameters obtained for the different kinetic

models (eq. S5-S8), including the power-law model (eq S2). The table includes the values of the parameters for each kinetic model, and the statistical parameter $\text{Var}(\text{SRR})$ used to compare them, and the regression coefficient (R^2) to evaluate the linearity of the parity plots in Figures S7-S8.

The excellent correspondence between the experimental and calculated values shows that models given by eqs. S2, S5 and S7, are very robust to predict low and high conversion levels, in a wide range of reaction conditions of T and W/F.

From the figures, is observed that the power law is as good as the models that took into account mechanistic considerations. While, in contrast with the mechanistic models, the power law-based equation is by far the simplest one.

Another observation based on the results shown in the Figure S7, is that when considering mechanistic-based models it is much better to assume that all the species present at the catalyst surface are kinetically relevant, and that the assumption that there are few species considered as the most abundant ones (such as eqs. S6 and S8), is not a good simplification.

The above results indicate that using mechanistically based models to fit the experimental kinetic data, is not providing enough evidence to draw conclusions related to the limiting step, since very similar fittings are obtained with the models considered here assuming different rate determining steps. The ability to fit experimental data does not constitute rigorous evidence to support a proposed reaction mechanism or kinetic model. That is the main reason why, in spite of the research over decades in this reaction, there is no agreement about which is the limiting step or the kinetically relevant surface species.

In order to check the validity of this models to predict the catalytic performance of ammonia decomposition reaction at high pressure, the different kinetic models with the parameters obtained as describe above, were used to calculate the conversion at high pressure and different temperatures. In the Figure S8, the parity plots comparing the experimental and calculated values. In red is shown the values for the conversion of ammonia at high pressure (those values were not used for the fitting in order to get the values of the parameters). The Figure S8 shows that models given by eqs. S2, S5 and S7, are very robust to predict data at high pressure. Specially the power law fitting here is slightly better than the mechanistic models even.

The equation considering that all the species can be relevant fit better the experimental results at high pressure. Of course, this would be even much more important at high pressure. So, the simplified eqs. S6 and S8 are the worst models, especially when intending to predict data at high pressure.

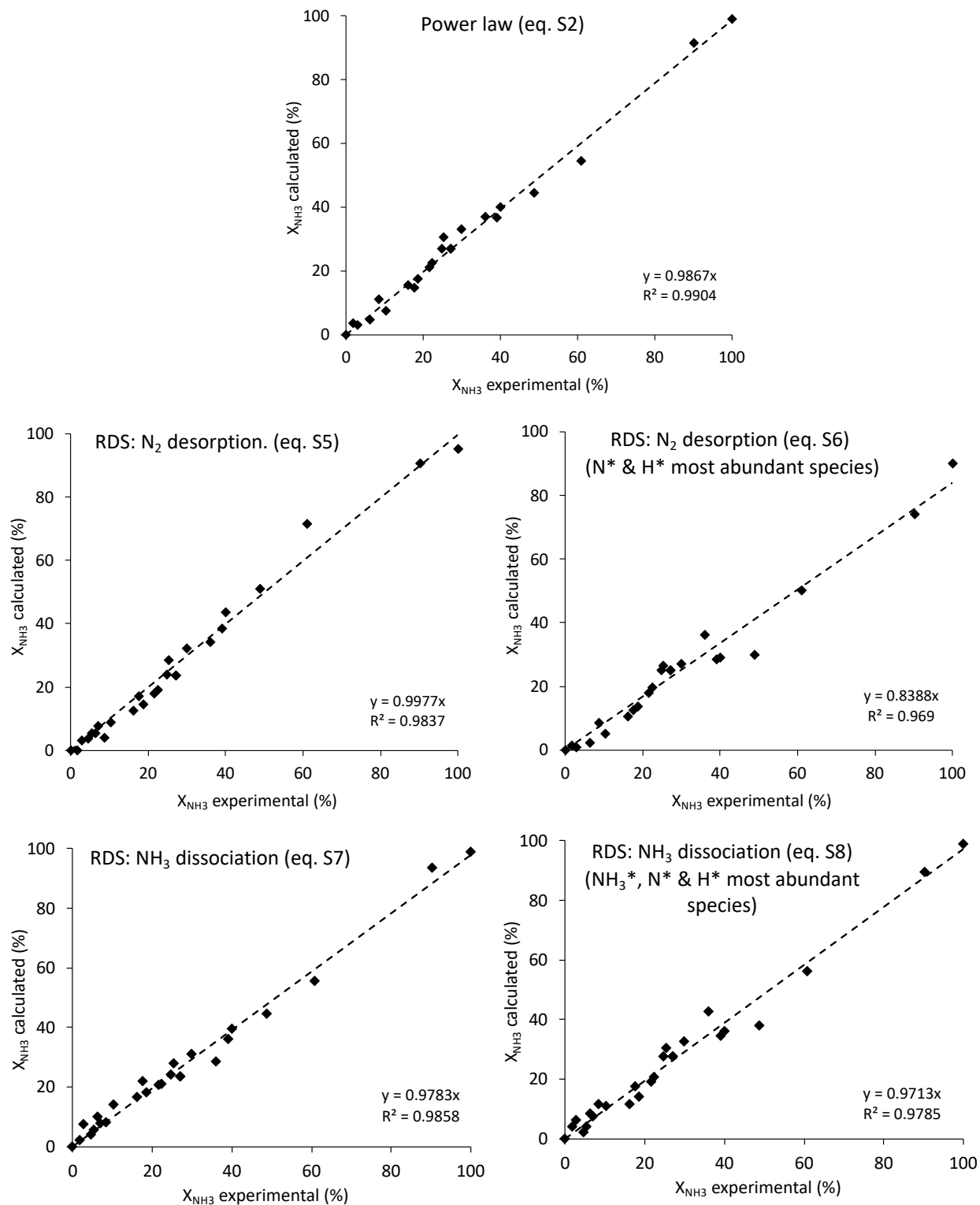


Figure S7. Parity plots comparing experimental vs. calculated ammonia conversion for 3%Ru-10%K/CaO catalyst using the kinetic models given by eq. S2, and eqs.S5-S8.

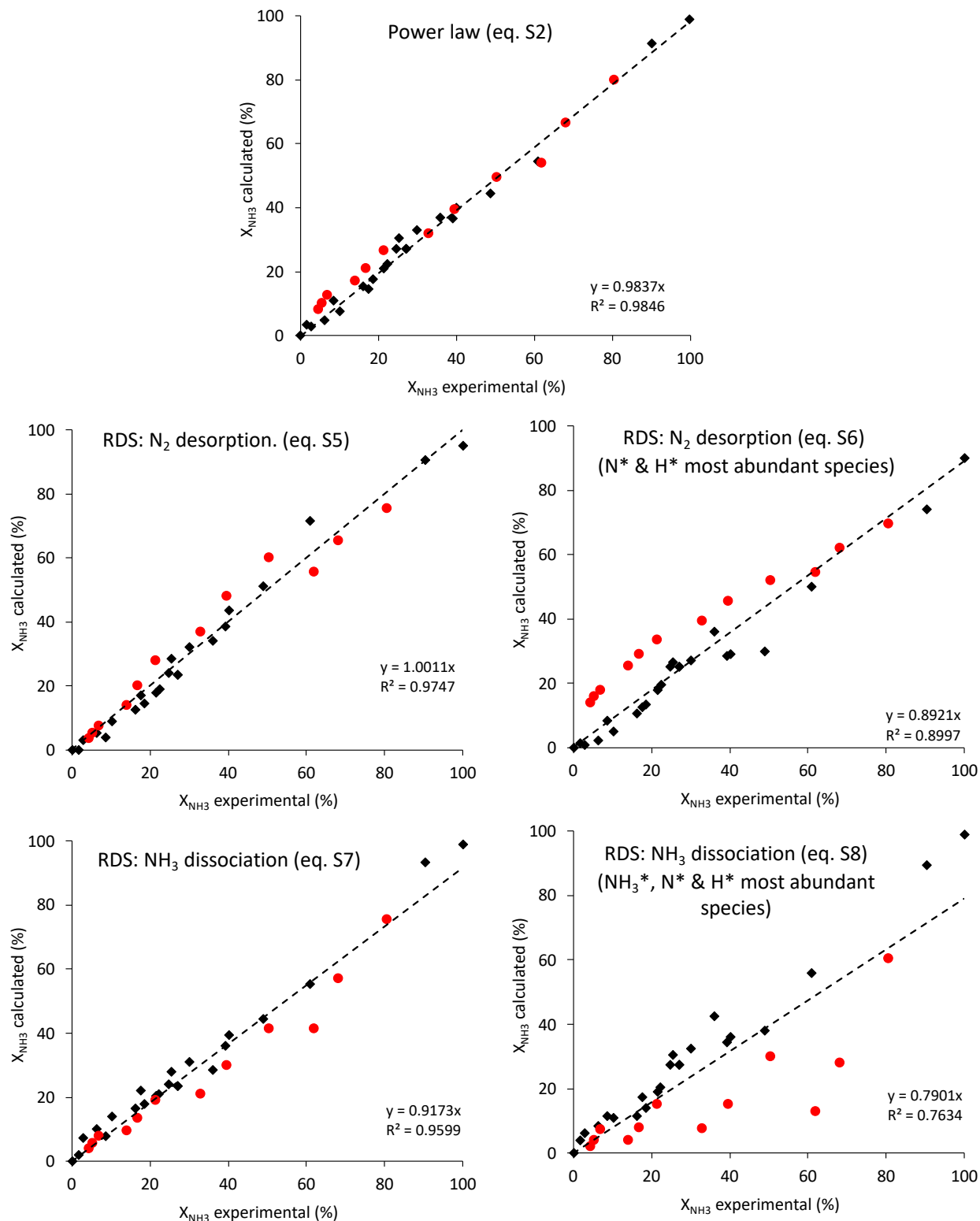


Figure S8. Experimental vs. calculated ammonia conversion using the kinetic models given by eq.S2, and eqs.S5-S8. for high pressure ammonia decomposition over 3%Ru-10%K/CaO catalyst. In red the values for the conversion of ammonia at high pressure (not used for the fitting). In black values of conversion at atmospheric pressure used for the fitting to get kinetic parameters.

The term included to calculate the net reaction rates that considers the approximation to the thermodynamic equilibrium (eq. S10) is evaluated at different pressure and temperatures in the Figure S9.

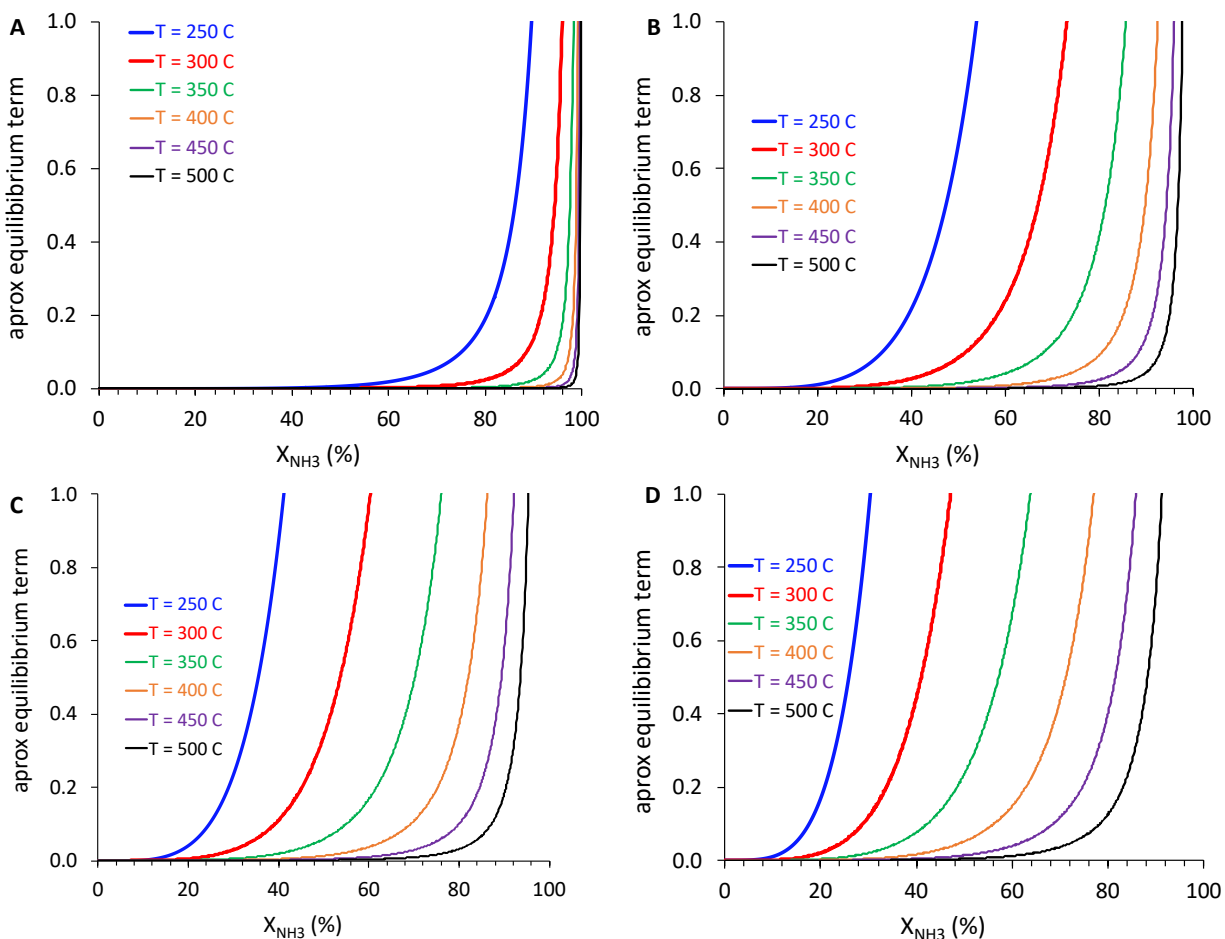


Figure S9. Values of the approximation to the thermodynamic equilibrium term that accounts the reverse reaction contribution. A) P=1bar, B) P=10 bar, C) P=20 bar and D) P=40 bar.

Summary of the kinetic parameters for the models given by equations S2 and S5-S8, in the Tables S4-S8.

Table S5. Kinetic parameters for the power law model (eq S2).

$(-r_{NH_3}) = k \times P_{NH_3}^a P_{H_2}^b \left(1 - \frac{1}{K_{eq}} \left(\frac{P_{N_2} P_{H_2}^3}{P_{NH_3}^2} \right) \right)$	
parameters	Ru-K/CaO
k_0 (mol g _{cat} ⁻¹ s ⁻¹)	8584.8
E_a (kJ mol ⁻¹)	111.0
a	0.5
b	-1.2
SSR	202
Var (SSR)	0.031
R ²	0.99

Table S6. Kinetic parameters for the model that considers desorption of nitrogen as the rate determining step (eqS5)

RDS: N₂ desorption	
$(-r_{NH_3}) = \frac{k_A K_{NH_3}^2 P_{NH_3}^2}{\left(K_{H_2}^{3/2} P_{H_2}^{3/2} (1 + \sqrt{K_{H_2} P_{H_2}}) + K_{NH_3} P_{NH_3} \left(1 + \frac{\sqrt{K_{H_2} P_{H_2}}}{K_3} \left(1 + \frac{\sqrt{K_{H_2} P_{H_2}}}{K_2} \left(1 + \frac{\sqrt{K_{H_2} P_{H_2}}}{K_1} \right) \right) \right) \right)^2}$	
parameters	3%Ru-15%K/CaO catalyst
$k_{A,0}$ (mol g _{cat} ⁻¹ s ⁻¹)	53656.9
E_a (kJ mol ⁻¹)	82.9
$K_{NH_3,0}$ (atm ⁻¹)×10 ⁻³	38.0
Q_{NH_3} (kJ mol ⁻¹)	130.2
$K_{H_2,0}$ (atm ⁻¹) ×10 ⁻³	11.6
Q_{H_2} (kJ mol ⁻¹)	93.7
$K_{1,0}$ (atm ⁻¹) ×10 ⁻³	70.7
Q_1 (kJ mol ⁻¹)	58.3
$K_{2,0}$ (atm ⁻¹) ×10 ⁻³	5.2
Q_2 (kJ mol ⁻¹)	6.2
$K_{3,0}$ (atm ⁻¹) ×10 ⁻³	91.7
Q_3 (kJ mol ⁻¹)	100.4
SSR	266
Var (SSR)	0.047
R ²	0.98

Table S7. Kinetic parameters for the model that considers desorption of nitrogen as the rate determining step, and N* and H* as the most abundant species. (eq S6)

RDS: N₂ desorption, and N* as the most abundant species	
$(-r_{NH_3}) = \frac{k_A K_{NH_3}^2 P_{NH_3}^2}{\left(K_{NH_3} P_{NH_3} + K_{H_2}^{3/2} P_{H_2}^{3/2} (1 + \sqrt{K_{H_2} P_{H_2}}) \right)^2}$	
parameters	3%Ru-15%K/CaO catalyst
$k_{A,0}$ (mol g _{cat} ⁻¹ s ⁻¹)	267.1
E_a (kJ mol ⁻¹)	81.3
$K_{NH_3,0}$ (atm ⁻¹) ×10 ⁻³	8.4
Q_{NH_3} (kJ mol ⁻¹)	123.3
$K_{H_2,0}$ (atm ⁻¹) ×10 ⁻³	0.0
Q_{H_2} (kJ mol ⁻¹)	62.7
SSR	1099
Var (SSR)	0.078
R ²	0.94

Table S8. Kinetic parameters for the model that considers ammonia dissociation as the rate determining step. (eqS7)

RDS: NH₃ dissociation	
$(-r_{NH_3}) = \frac{k_B K_{NH_3} P_{NH_3}}{\left(1 + K_{NH_3} P_{NH_3} + \sqrt{K_{H_2} P_{H_2}} + \sqrt{K_{N_2} P_{N_2}} \left(1 + \frac{\sqrt{K_{H_2} P_{H_2}}}{K_3} \left(1 + \frac{\sqrt{K_{H_2} P_{H_2}}}{K_2}\right)\right)\right)^2}$	
parameters	Ru-K/CaO
$K_{B,0}$ (mol g _{cat} ⁻¹ s ⁻¹)	28649.6
E_a (kJ mol ⁻¹)	50.2
$K_{NH_3,0}$ (atm ⁻¹) ×10 ⁻³	48.6
Q_{NH_3} (kJ mol ⁻¹)	77.1
$K_{H_2,0}$ (atm ⁻¹) ×10 ⁻³	30.7
Q_{H_2} (kJ mol ⁻¹)	36.4
$K_{N_2,0}$ (atm ⁻¹) ×10 ⁻³	35.6
Q_{N_2} (kJ mol ⁻¹)	31.7
$K_{2,0}$ (atm ⁻¹) ×10 ⁻³	77.3
Q_2 (kJ mol ⁻¹)	70.3
$K_{3,0}$ (atm ⁻¹) ×10 ⁻³	19.3
Q_3 (kJ mol ⁻¹)	42.7
SSR	219
Var (SSR)	0.042
R ²	0.98

Table S9. Kinetic parameters for the model that considers ammonia dissociation as the rate determining step, and NH₃^{*}, H^{*} and N^{*} as the most abundant species. (eq. S8)

RDS: NH₃ dissociation, and NH₃[*], H[*] and N[*] as the most abundant species	
$(-r_{NH_3}) = \frac{k_B K_{NH_3} P_{NH_3}}{\left(1 + K_{NH_3} P_{NH_3} + \sqrt{K_{H_2} P_{H_2}} + \sqrt{K_{N_2} P_{N_2}}\right)^2}$	
parameters	Ru-K/CaO
$K_{B,0}$ (mol g _{cat} ⁻¹ s ⁻¹)	16817.1
E_a (kJ mol ⁻¹)	75.1
$K_{NH_3,0}$ (atm ⁻¹) ×10 ⁻³	24.7
Q_{NH_3} (kJ mol ⁻¹)	28.9
$K_{H_2,0}$ (atm ⁻¹) ×10 ⁻³	44.6
Q_{H_2} (kJ mol ⁻¹)	2.0
$K_{N_2,0}$ (atm ⁻¹) ×10 ⁻³	37.1
Q_{N_2} (kJ mol ⁻¹)	82.0
SSR	353
Var (SSR)	0.046
R ²	0.97

¹ Armenise, S.; García-Bordejé, E.; Valverde, J. L.; Romeo, E.; Monzón, A., A Langmuir–Hinshelwood approach to the kinetic modelling of catalytic ammonia decomposition in an integral reactor. *Physical Chemistry Chemical Physics* **2013**, *15* (29), 12104-12117.

² Introduction to Chemical Engineering Thermodynamics, ed. J. M. Smith, H. Van Ness and M. Abbott, The McGraw-Hill Chemical Engineering Series, United States, November 12, 2004 edn, 2004.